Post-quench ductility limits of coated ATF with various zirconium-based alloys and coating designs

SungHoon Joung [a], Jinsu Kim [b], Martin Ševeček [c], Juri Stuckert [d], Youho Lee [a,*]

[a] Department of Nuclear Engineering, Seoul National University, Gwanak-ro 1, Gwanak-gu, Seoul 08826, Republic of Korea
[b] Nuclear Research Institute for Future Technology and Policy, Seoul National University, Gwanak-ro 1, Gwanak-gu, Seoul 08826, Republic of Korea
[c] Faculty of Nuclear Sciences and Physical Engineering, Czech Technical University in Prague, Prague, Czech Republic
[d] Institute for Applied Materials IAM-AWP, Karlsruhe Institute of Technology, 76021 Karlsruhe, Germany

Keywords:
Accident tolerant fuel (ATF)
Cr-coated cladding
Post quench ductility
ECCS criteria
Failure mode

A B S T R A C T

Post Quench Ductility (PQD) of various Cr-coated cladding designs with respect to base cladding materials, Cr coating methods, and its thickness were investigated to explore Emergency Core Cooling System (ECCS) limits. Both inner wall and outer wall of coated (Cr and Cr/CrN) claddings were steam oxidized at ~1204 °C and then water quenched. The post-oxidized specimens were ring compressed to attain offset strains based on which ductility was assessed in compliance with the U.S. Nuclear Regulatory Commission (U.S. NRC)'s protocols. Weight gain-based Equivalent Cladding Reacted (ECR) limits of coated specimens (Cr and Cr/CrN) are consistently lower than those of the base cladding materials due to the early load drop under Ring Compression Test (RCT). Yet, time needed to reach the ECR limit is still increased for coated specimens because it effectively undergoes single side oxidation with protective coating. Cracks imitated from $ZrCr_2$ are primarily responsible for the early major load drop observed for tested coating thicknesses (8.9 μm and 18.9 μm), and hence reduced ECR limits compared to bare Zircaloy. The cracks from $ZrCr_2$ was promoted by an increased oxygen concentration of the interfacing Zr matrix owing to the diffusion of oxygen through the coating. The thicker coating reduces this oxygen level, thereby delaying the load drop from $ZrCr_2$ during RCT and increases the ECR limit. The maximum attainable ECR limit of coated ECR limits is affected by the base Zircaloy as it gives as the ECR ceiling from which ECR reduction for coated cladding occurs. For the tested base cladding materials (Opt. ZIRLO™ and HANA-6), ECR 19 %, which is the limit for Cr-coated (8.9 μm) HANA-6, may serve as the lower envelope limit. Hence, ECR 19 % (single-side ECR) can conservatively serve as the conservative, yet non-design specific, Cr-coated ECR limit for the most of the modern base Zircaloy materials (Opt. ZIRLO™ and HANA-6).

1. Introduction

Ensuring the mechanical integrity of cladding is critical for the safety of nuclear fuel. However, during a Loss Of Coolant Accident (LOCA) situation, the cladding specimens experience high-temperature steam oxidation, resulting in a considerable reduction in ductility due to oxygen and hydrogen pickup. As such, post-LOCA ductility of Zircaloy cladding has served as a critical basis of safety assurance criteria for Emergency Core Cooling Systems (ECCS) in many countries such as United States of America (USA) and Republic of Korea (ROK). The U.S. Nuclear Regulatory Commission (U.S. NRC) established experimental protocols to test post-LOCA ductility of Zircaloy claddings subjected to high temperature oxidation and subsequent reflood water quench [1]. The current ECCS criteria (i.e., 10 CFR 50.46 of U.S. NRC) limit Peak Cladding Temperature (PCT) and Equivalent Cladding Reacted (ECR) to 1204 °C and 17 %, respectively [2,3].

In the midst of it, the concept of Accident Tolerant Fuel (ATF) cladding was proposed in response to Fukushima accidents. Most ATF cladding concepts aim to significantly suppress cladding steam oxidation in the pursuit of extending the accident coping time while maintaining desirable thermal performance and mechanical integrity. Among the number of ATF concepts, Cr-coated Zircaloy cladding is considered as a promising concept under development for near-term commercialization [4]. Cr-coated Zircaloy cladding exhibits orders of magnitudes slower oxidation rates compared to Zircaloy, and presents minimum departure from the current cladding material thereby facilitating timely

* Corresponding author.
E-mail address: leeyouho@snu.ac.kr (Y. Lee).

commercialization with expedited fuel testing, qualification, and licensing compared to other ATFs [5].

Design Basis Accident (DBA) safety limits of Cr-coated ATF remain as a critical knowledge gap for its commercialization, licensing, and performance evaluation. Not only is it required for regulation, but it would also reveal the extent of accident coping time when applied to safety analysis. The primary performance using metallic Zircaloy as the base material, it is reasonable to anticipate that the ECCS criteria of Cr-coated Zircaloy may as well comply with the Post-Quench Ductility (PQD) assessments applied to the Zircaloy cladding. In line with this, the Interim Staff Guideline (ISG) published by the U.S. NRC states, '*Hence, the applicability of the 17-percent equivalent cladding reacted analytical limit and, more generally, the use of maximum local oxidation as a surrogate SAFDL for cladding embrittlement is questionable*' [6]. From this guideline, one can infer that the post-quench ductility (PQD) of Cr-coated cladding, conducted in compliance with the current experimental protocols, would provide a critical basis for assessing the potential deviations from or adherence to current limits.

Yook et al. [7] led the efforts of exploring the ECCS limits of Cr-coated cladding obtained by applying the U.S. NRC's PQD test protocols. The study concluded that the inner side oxidation of Cr-coated Zircaloy near the burst hole is the limiting DBA phenomenon in Large Break Loss of Coolant Accidents (LBLOCA), and presents the single side oxidation limit of ECR ~14 % for peak cladding temperature of 1204 °C for the tested Cr-coated specimens. The decrease in the ECR limit from the current value of 17 % is owing to single side oxidation of Cr-coated Zircaloy which results in the thicker inner-side oxide and oxygen rich α(o) phase compared to the bare Zircaloy for the same ECR. The study highlights that the accident coping time for Cr-coated Zircaloy nevertheless increases, yet to a limited extent, thanks to single side oxidation. It is noteworthy that it used Zircaloy-4 specimens with Cr-coating thickness of 39.4 μm deposited by cold spray. The validity of the derived ECR limits for various base cladding types (i.e., Zircaloy-4, Zirlo, Opt. ZIRLO™, and HANA-6), and coating methods and thickness remain to be investigated. Extensive assessments of PQD limits for various coated-Zircaloy designs will provide a critical basis to the development of ATF regulatory framework (i.e., universal PQD limits vs design-specific PQD limits) and design implications.

This study presents PQD assessments of various Cr-coated cladding designs with respect to base cladding materials, Cr coating methods, and their thickness. The results are further investigated with microstructural analyses and regulatory implications are discussed.

2. Experimental setup

2.1. Materials

The PQD experiment was performed in this work employing various cladding materials, including bare Zircaloy-4 (14 × 14), Opt. ZIRLO™, and HANA-6 alloy. To evaluate the residual ductility of the coated ATF after oxidation in a high temperature steam environment and water quenching, reactor-grade chromium-coated Zircaloy-4, Opt. ZIRLO™, and HANA-6 claddings were prepared. A Cr/CrN bi-layer coated Opt. ZIRLO™ cladding was also tested. Arc Ion Plating (AIP) was employed to deposit Cr coating on HANA-6 cladding at a temperature exceeding 500 °C. Magnetron sputtering was used to coat Opt. ZIRLO™ cladding with Cr and Cr/CrN at an average sample temperature of around 280 °C. Cr coated Zircaloy-4 was also prepared using magnetron sputtering at 270 °C, with no observed recrystallization in the cladding. Table 1 lists the dimensions of all claddings, including their outer diameter (OD), thickness and the compositions. Coating thicknesses for each specimen was evaluated using Scanning Electron Microscope (SEM).

The claddings specimens were machined to an 8 mm length for the PQD experiment. Any burrs formed during the machining process were removed to measure the correct weight of the claddings. Fig. 1 shows cross-sectional images of the as-received specimens. The Cr or CrN coating on all of the specimens has a dense appearance without micro-voids and micro-cracks, as shown in Fig. 1. Additionally, both Cr and CrN coatings have a fairly uniform thickness throughout the surface.

2.2. PQD experiments

For the PQD experimental procedure, this study followed the experimental protocol provided by the U.S. Nuclear Regulatory Commission (U.S. NRC) [1,8]. The specimens were cleaned with ethanol and de-ionized water before oxidation to remove any impurities. The weight of each specimen was measured using a balance with a precision of 0.0001 g after complete drying to remove residual moisture.

Following the weight measurement, the specimens were placed in a holder and exposed to a high-temperature steam environment, as illustrated in Fig. 2(a). The experimental equipment highlighted in Fig. 2(a) has been extensively validated by a number of previous studies [7,9-12]. A *K*-type thermocouple was attached to a dummy specimen which is held in the sample holder during the steam oxidation process to measure the temperature of the specimens. The temperature history of the specimens is shown in Fig. 2(b) during the oxidation process. The temperature of the specimens was maintained to be 1204 ± 5 °C during 120 s to 2400 s corresponding to the area of interest in ECR, and the steam flow rate was set to be 3.94 mg/cm^2 s. This flow rate is within the recommended range provided by the U.S. NRC to prevent steam starvation

Table 1
The nomenclature, coating method, chemical composition, and dimensional characteristics of the various coated claddings examined in this study.

Alloy	Coating method	Nb	Sn	Fe	Cr	Cu	Outer radius (mm)	Thickness (δ) (mm)	Coating thickness (μm)
Zircaloy-4	Bare Cladding	–	1.3–1.5	0.2	0.1	–	10.75	0.75	–
	Cr (Magnetron)								9.2 ± 0.2
Opt. ZIRLO™	Bare cladding	1.0	0.7	0.12	–	–	9.15	0.57	–
	Cr (Magnetron)								18.8 ± 0.7
	Cr/CrN (Magnetron)								20.1 ± 0.4/7.3 ± 0.1
HANA-6	Bare cladding	1.1	–	–	–	0.05	9.5	0.57	–
	Cr (8.9 μm, AIP)								8.9 ± 0.6
	Cr (19.0 μm, AIP)								19.0 ± 0.3

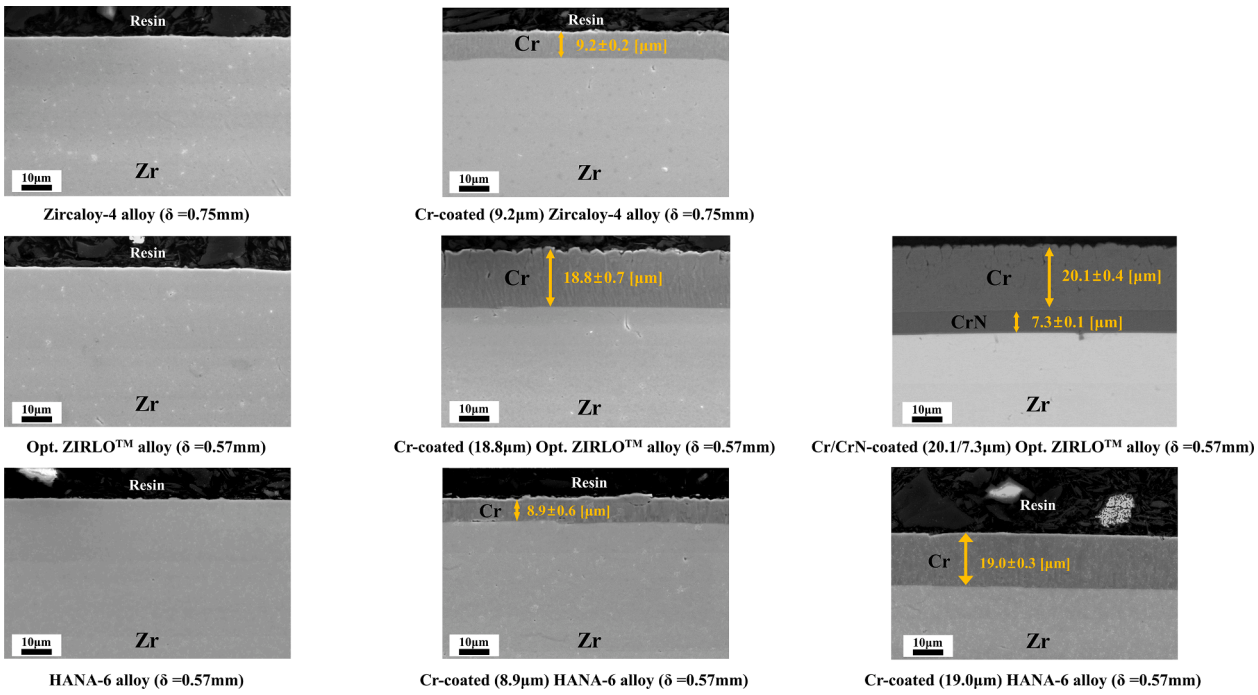

Fig. 1. Cross-sectional images of the as-received specimens.

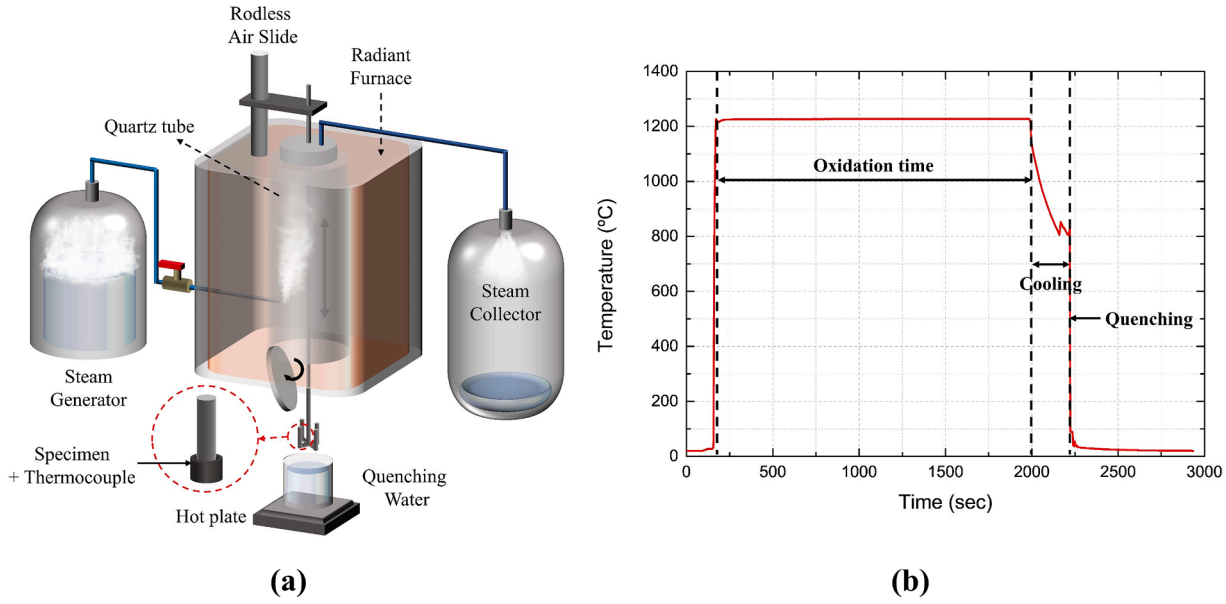

Fig. 2. LOCA experimental setup and temperature profile, (a) Schematic of LOCA simulated facility (b) Temperature profile during LOCA simulated experiment.

[13]. The oxidized specimens were cooled down to 800 °C at a rate ranging from 2 °C/s to 4 °C/s, by introducing an increased flow rate of steam and argon mixture. The steam to Ar mass flow rate is greater than 10. The specimens were quenched in boiling water after reaching 800 °C. The quenching of specimens in boiling water mimics the reflood quenching of the fuel rods upon the activation of ECCS injection. After the oxidation and quenching processes were completed, the specimens were cleaned with ethanol and de-ionized water. The specimens were thoroughly dried and re-weighed to calculate Weight Gain-Equivalent Cladding Reacted (WG-ECR). The WG-ECR was computed by the weight changes Δm with oxidation, as shown in Eq. (1). For coated specimens, Cr_2O_3 was formed due to the oxidation of Cr coating. Yet, the thin Cr_2O_3 layer has a minor effect less than 1.7 % of total weight gain for ECR 18 % (i.e., 1.7 % of 18 % ECR is ~0.3 %) at 1204 °C on mass change and thus it was excluded from the WG-ECR calculation.

$$\text{WG} \quad \text{ECR}[\%] = \frac{\Delta m}{2 \times \frac{M_O}{M_{Zr}} \times m_i \times f_{Zr}} \tag{1}$$

where Δm, M_O, M_{Zr}, m_i, f_{Zr} are difference of mass before and after the oxidation, molecular weight of oxygen, molecular weight of the zirconium, mass of the specimens before the oxidation, and fraction of the zirconium in alloy, respectively [14–16]. Note that the fraction of the zirconium of each type of cladding, f_{Zr}, was attained based on compositions given in Table 1. Additionally, the Zr fraction in the Cr-coated cladding is the same with its base cladding since weight gain

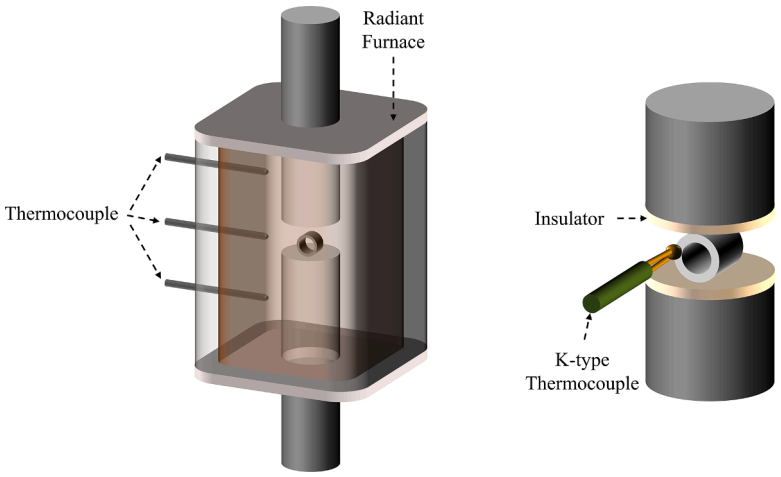

Fig. 3. Schematic of ring compression test facility.

predominantly (>98 %) arises from oxidation of Zircaloy.

After the oxidation process, the residual ductility of the oxidized specimens was evaluated via Ring Compression Test (RCT) by using universal testing machine (INSTRON-8516). A schematic diagram of RCT facility is shown in Fig. 3. Aluminum insulators were placed on both upper and lower compression rods to minimize the temperature gradient through azimuthal direction of the specimens. The temperatures of four different angular positions (3, 6, 9, 12′o clock) of the specimen were maintained within 135 ± 3 °C. The compression tests were performed at a strain rate of 0.033 mm/s, following the experimental protocol recommended by the U.S. NRC [13].

3. Results

The performance of steam oxidation facility was validated by comparing the experimentally obtained WG-ECR and ECR predicted by Cathcart–Pawel correlation (CP-ECR) as shown in Eq. (2) [17].

$$\begin{aligned} \text{Single} \quad \text{sideCP} \quad \text{ECR}[\%] &= 2.85 w_o/(\rho_{Zr} h_r) \\ \text{Double} \quad \text{side CP} \quad \text{ECR}[\%] &= 2 \times 2.85 w_o/(\rho_{Zr} h_r) \end{aligned} \tag{2}$$

$$w_o \ [\text{g}/\text{cm}^2] = \sqrt{0.3622\ t \exp\left(\frac{39,940}{1.987 \times T}\right)}$$

where w_o, ρ_{Zr}, h_r, t, T are weight-gain/surface-area due to oxygen pickup, density of Zircaloy, reference cladding thickness in cm, time in seconds and temperature in K, respectively. The measured temperature with the K-type thermocouple was used for the CP-ECR prediction. As shown in Fig. 4(a) and (b), the WG-ECR of various uncoated and coated Zircaloy specimens gives a good agreement with double-side CP-ECR and single-side CP-ECR predictions, respectively. Upon transformation from single-side oxidation into a double-sided oxidation ECR correlation, it involves multiplying by 2 [13]. However, in the case of coated cladding, the oxidation occurs predominantly on the inner surfaces, necessitating the consideration of their respective areas. To be precise, the CP-ECR correlation should be multiplied by 1.88 to account for the smaller area of the inner wall. The maximum error for uncoated specimens is within ~10 %, whereas the maximum error for coated specimens is ~12 %. As can be inferred, predictability of one-side CP-ECR (Fig. 4(b)) for uncoated Zircaloy demonstrates that no appreciable loss of coating protectiveness occurred in the tested periods of time, and similar results were reported in past studies [7]. These results demonstrate the sanity of oxidation facility and specimen temperature measurements during the oxidation process.

Fig. 5 illustrates a load-displacement curve obtained from the RCT. The initial stage of the RCT is considered the elastic region, and the Pseudo Stiffness of the material is determined by calculating the slope at

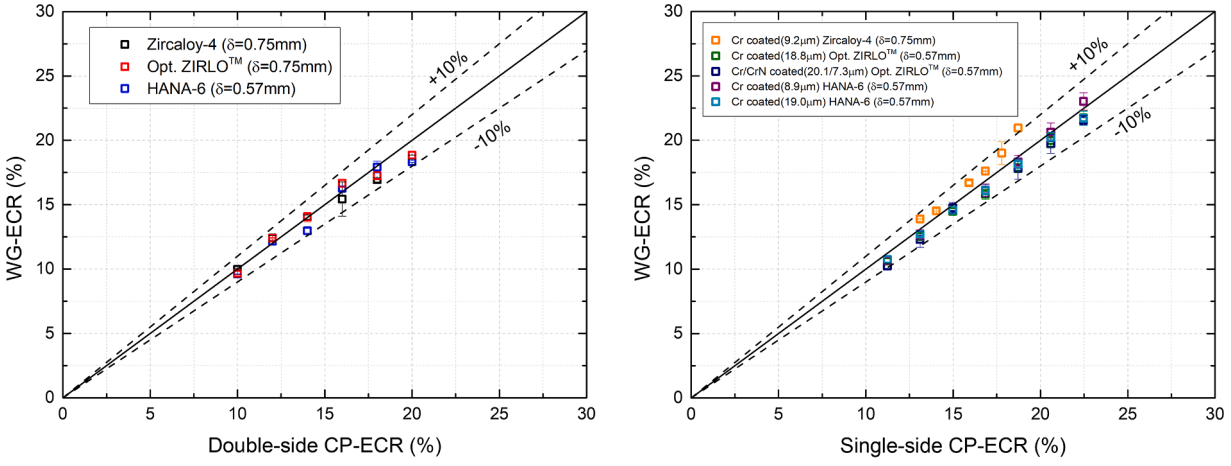

Fig. 4. WG-ECR according to time for various specimens (a) no coated specimens (b) coated specimens.

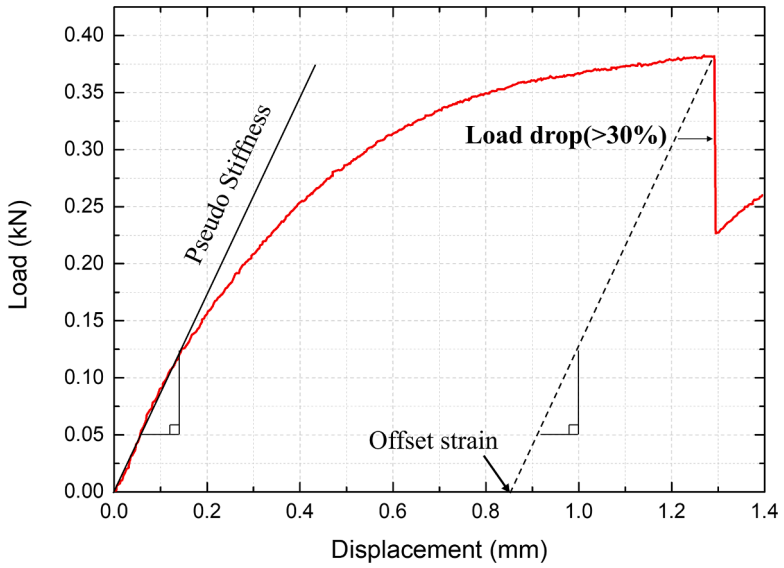

Fig. 5. A load-displacement curve and parameters obtained from RCT.

this initial stage. The offset strain is subsequently calculated using the displacement and load values at the point of load drop, which is defined as a sudden load decrease exceeding 30 %. At this point, it is assumed that a crack propagates across the entire thickness of the specimen [1], which is referred to as a through-wall crack from hereafter in this paper.

Following the methodology recommended by the U.S. NRC, offset strain (%), which is obtained by dividing the displacement by the outer diameter of the pre-oxidized specimens and multiplied by 100, was utilized to assess the residual ductility of the specimens [13]. Offset strain of Zircaloy-4 (δ = 0.57 mm) with WG-EGR was obtained to validate the experiments with the U.S. NRC's past results. The result exhibits remarkable agreement with that of U.S. NRC's experimental data (Fig. A of Appendix), validating the conducted experiments including steam oxidation, water quenching, and RCT. Fig. 6 presents the offset strains of all uncoated and coated specimens based on WG-ECR. The ductility of the specimens decreases as the amount of the oxidation increases. A WG-ECR limit is calculated by finding an intersection point between the ductile to brittle transition line proposed by U. S. NRC [1], which is shown as black linear line in each graph of Fig. 6, and the fitted curve of experimental data (dashed line). Note that the experimental data was fitted by using a functional form of $y = a \quad bc^x$, where x and y are the WG-ECR(%) and the offset strain (%), respectively. The a, b, and c are fitting constants for each cladding. The selected fitting function effectively represents the data trend with high R^2 values (range: 0.83–0.92) for all tested claddings. This form of equation was also used in a past study [7].

Table 2 provides a summary of the ductile to brittle transition WG-ECR limits obtained from Fig. 6. It shows that the WG-ECR limits of coated specimens (Cr and Cr/CrN) are consistently lower than those of the base cladding materials. Based on the WG-ECR limit, the reduction ranges from a maximum of 5 % (ΔECR) to a minimum of 1 % (ΔECR). Hence, bare Zircaloys serve as the ECR ceiling from which ECR reduction for coated cladding occurs. Nevertheless, caution should be taken so as not to misinterpret the result; time needed to reach the ECR limit is still increased for coated specimens because of single-side oxidation. As can be noted in HANA-6 data (Table 2), the thinner coating results in a lower WG-ECR limit (19 % for 8.9 μm) compared to the thicker coating (22 % for 19.0 μm), demonstrating a notable level of coating thickness sensitivity.

The reduction of the ECR limit for Cr-coated specimens was also reported elsewhere [7,18,19]. Yook et al. [7] explained that the reduced ECR limit for Cr-coated specimen is due to single-side oxidation of Cr-coated Zircaloy. This results in the thicker inner-side oxide (ZrO_2) and oxygen rich α(o) phase compared to the bare zircaloy, making it more prone to developing cracks under RCT. It used Zircaloy-4 specimens with Cr coating thickness of ~40 μm deposited by cold spray. The deposited coating is unusually thicker than most Cr coating thicknesses under consideration for commercialization. The validity of the derived ECR limits of Yook et al. [7] for various base cladding types (i.e., Zircaloy-4, Opt. ZIRLO™, and HANA-6), and coating methods and thickness remain to be investigated. Indeed, the proposed mechanism for the reduced ECR limit of Cr-coated specimens cannot explain the present sensitivity of coating thickness; the thicknesses of inner side ZrO_2 and oxygen rich α(o) phase are insensitive to the outer coating thickness. This may call for revisiting the current understanding of the reduced ECR limits for Cr-coated cladding under RCT and developing a universally working explanation for various Cr-coated Zircaloy cladding designs.

In order to develop a unifying explanation for the decreased ECR limits consistently observed for all tested Cr-coated specimens and the coating thickness sensitivity, this study conducted an extensive in-depth investigation for the failure modes of the tested specimens in RCT in conjunction with microstructural and oxygen distribution analysis.

In addition, we conducted SEM analysis of the claddings after oxidation. From the SEM images, as can be noted in Fig. C in Appendix, thickness of ZrO_2 at the inner wall can be readily measured and is reported in Table 2. $ZrCr_2$ layer was observable in SEM and its thicknesses were measured. 60 different locations were analyzed for inner ZrO_2, $ZrCr_2$, and Cr thickness, and their average and standard deviations are summarized in Table 2. Thickness of ZrO_2 was compared with prediction of TRANOX-2.0 [11], and they are in good agreement as shown in Fig. D in Appendix. TRANOX also accurately predicted the thickness of the inner wall Zr-alpha(O) obtained by EPMA. As can be inferred from Fig. C, the boundary delineating Zr-alpha(O) phase and prior-β is not clear under SEM. Hence, the thickness of the inner Zr-alpha(O) was obtained from TRANOX which was demonstrated to accurately predict the inner wall Zr-alpha(O) phase in this study (Fig. D in Appendix) and elsewhere [7]. The integrity of Cr_2O_3 was not maintained for tested

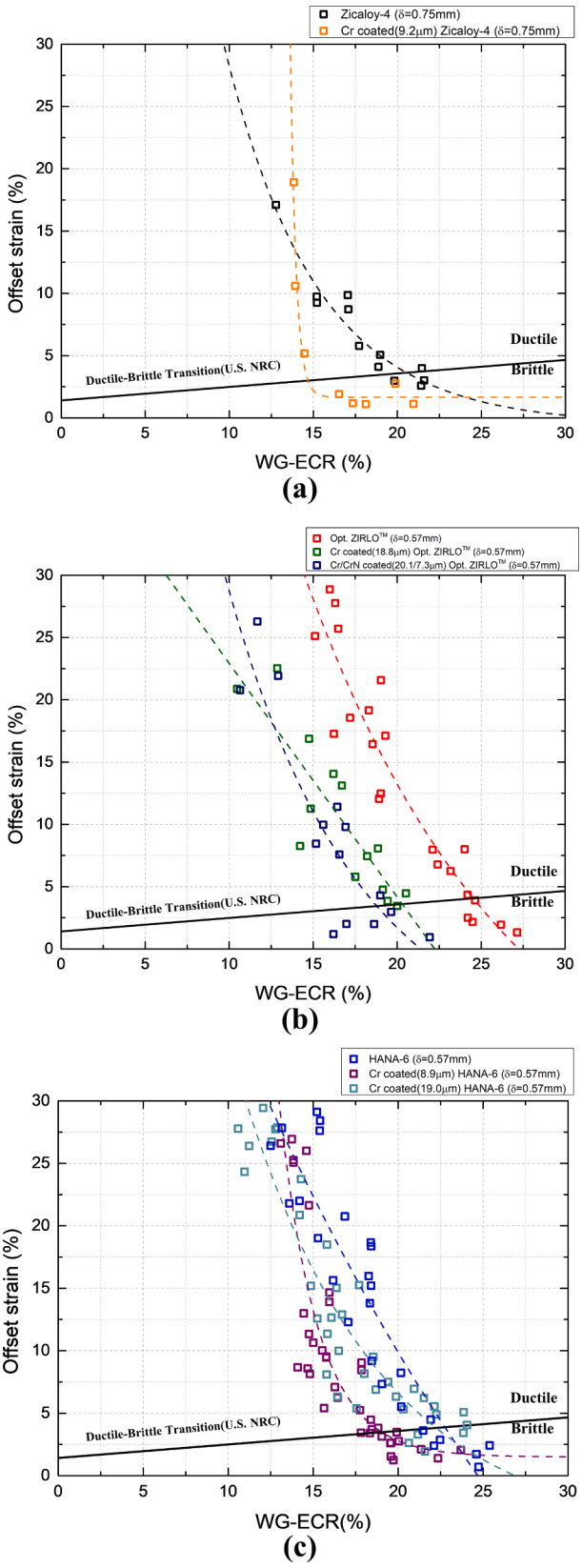

Fig. 6. WG-ECR to offset strain curve with ductile to brittle criteria from U.S. NRC. (a) Cr coating on Zircaloy-4 base material (b) Cr and Cr/CrN coating on Opt. ZIRLO™ base material (c) Cr coating on HANA-6 base material.

materials after hot mounting, and it is not the subject of investigation in this study.

4. Discussion

4.1. A general mechanism for reduced ECR limits of C- coated cladding

The experimental results revealed that post-LOCA ductility of coated cladding was lower than that of uncoated cladding for the same ECR. In order to elucidate it, characteristics of crack propagation under RCT was investigated using Digital Image Correlation (DIC). Fig. 7(a-1) and (a-2) show the initial crack and the major (through-wall) crack responsible for major load drop, respectively. Cr-coated specimens with ECR values near the brittle limit were chosen to make the case relevant to the reduced ECR limits. For all tested uncoated claddings, cracks initiated at either 6 o'clock or 12 o'clock position and these cracks further developed into major cracks which were responsible for the major load drop in RCT. These positions correspond to the location of maximum tensile stresses under RCT for specimens whose geometry still maintains a fairly cylindrical shape during deformation [20]. Finite Element Analysis (FEA) for RCT also indicates that the maximum tensile stress occurs at 6 o'clock or 12 o'clock position even with a slight departure from the original cylindrical shape after some deformation (See Appendix B). It is noteworthy that the typical ECR limit ranges (15–20 %) entail cylindrical shape of the specimen at the moment of fracture under RCT without much ductility which would have otherwise resulted in the peanut-shape by accommodating extended deformation. Consequently, for uncoated post-LOCA claddings, the maximum tensile acts on the most brittle phase (ZrO_2 and neighboring $\alpha(o)$ phase at the inner surface), and it results in crack propagation at 6 o'clock or 12 o'clock positions. This result is consistent with a past study investigating the characteristics of crack propagation in Zircaloy during RCT [7].

A different crack behavior was observed for the coated claddings. Similar to the uncoated cladding, cracks start to initiate at the inner surface of either 6 o'clock or 12o'clock positions where maximum tensile stresses act on brittle phases. However, as the coated cladding deformation proceeds under RCT, the major crack develops at either 3 o'clock and 9 o'clock positions as shown in Fig. 7(b-2). This behavior was consistently observed in all types of coated claddings tested in this study. This implies that the initial crack developed from the brittle phases of inner wall does not grow into the major crack, but instead it is likely to be arrested in the Zircaloy matrix and a different crack either from 3 o'clock or 9 o'clock grows into a through-wall crack. Hence, those cracks developed from 3 o'clock or 9 o'clock lead to the major load drop, and is thereby responsible for the present decrease in the ECR limit of Cr -coated claddings.

The observed crack characteristics were further investigated by SEM and Electron Probe Micro-Analyzer (EPMA) analysis. Fig. 8 shows the notable crack morphologies right before and after the major load drop for Cr-coated (19.0 μm) HANA-6 near the ECR limit (~20 %). Right before the major load drop, two different types of arrested cracks were observed: relatively thick and large cracks at 6′o clock and 12′o clock, and thin cracks near 3′o clock and 9′o clock. As can be seen, the cracks developed at 6′o clock and 12′o clock initiated from the brittle phases (ZrO_2 and $\alpha(o)$ phase). In the meantime, small cracks were also developed at 3′o clock and 9′o clock. These cracks extended from the thin $ZrCr_2$ layer to the outermost surface of Cr layer as discussed in Section 4.2 in detail. No porosity was observed at the Zr/Cr interface. Because Cr diffusion in Zr is interstitial [21], no appreciable Kirkendal effect was present. The pronounced embrittlement at the Zr/Cr interface is therefore primarily due to oxygen-induced solid solution hardening and diffused Cr in Zr which precipitates as $ZrCr_2$ after high temperature exposure. Upon further strain under RCT, the thin cracks at 3′o clock and 9′o clock undergo unstable through-wall crack propagation, which leads to the major load drop. As can be noted in Fig. B in Appendix A, the outer

Table 2
Ductile to brittle transition WG-ECR limit and thickness of each layer.

Base material	Coating	WG-ECR limit (%)	Inner ZrO_2 (μm)		Inner Zr-alpha (O) (μm)		Cr after oxidation (μm)	$ZrCr_2$ (μm)
			EXP.	TRANOX [11]	EXP.	TRANOX [11]		
Zircaloy-4 ($\delta = 0.75$ mm)	Bare cladding	20	75.2 ± 1.3	73.4	–	61.5	–	–
	Cr (9.2 μm)	15	100.3 ± 1.1	111.3	–	116.2	4.8 ± 0.5	1.3 ± 0.3
Opt. ZIRLO™ ($\delta = 0.57$ mm)	Bare cladding	24	64.7 ± 0.3	67.4	–	56.2	–	–
	Cr (18.8 μm)	20	116.9 ± 1.7	113.1	–	117.5	15.8 ± 0.4	0.9 ± 0.2
	Cr/CrN (20.1/7.3 μm)	19	116.0 ± 0.8	107.5	–	111.5	25.7 ± 0.7	1.1 ± 0.2
HANA-6 ($\delta = 0.57$ mm)	Bare cladding	23	71.2 ± 0.5	64.7	–	54.2	–	–
	Cr (8.9 μm)	19	105.7 ± 0.7	107.5	–	111.5	4.0 ± 0.5	0.8 ± 0.2
	Cr (19.0 μm)	22	112.5 ± 1.5	124.5	–	130.0	14.1 ± 0.5	1.0 ± 0.2

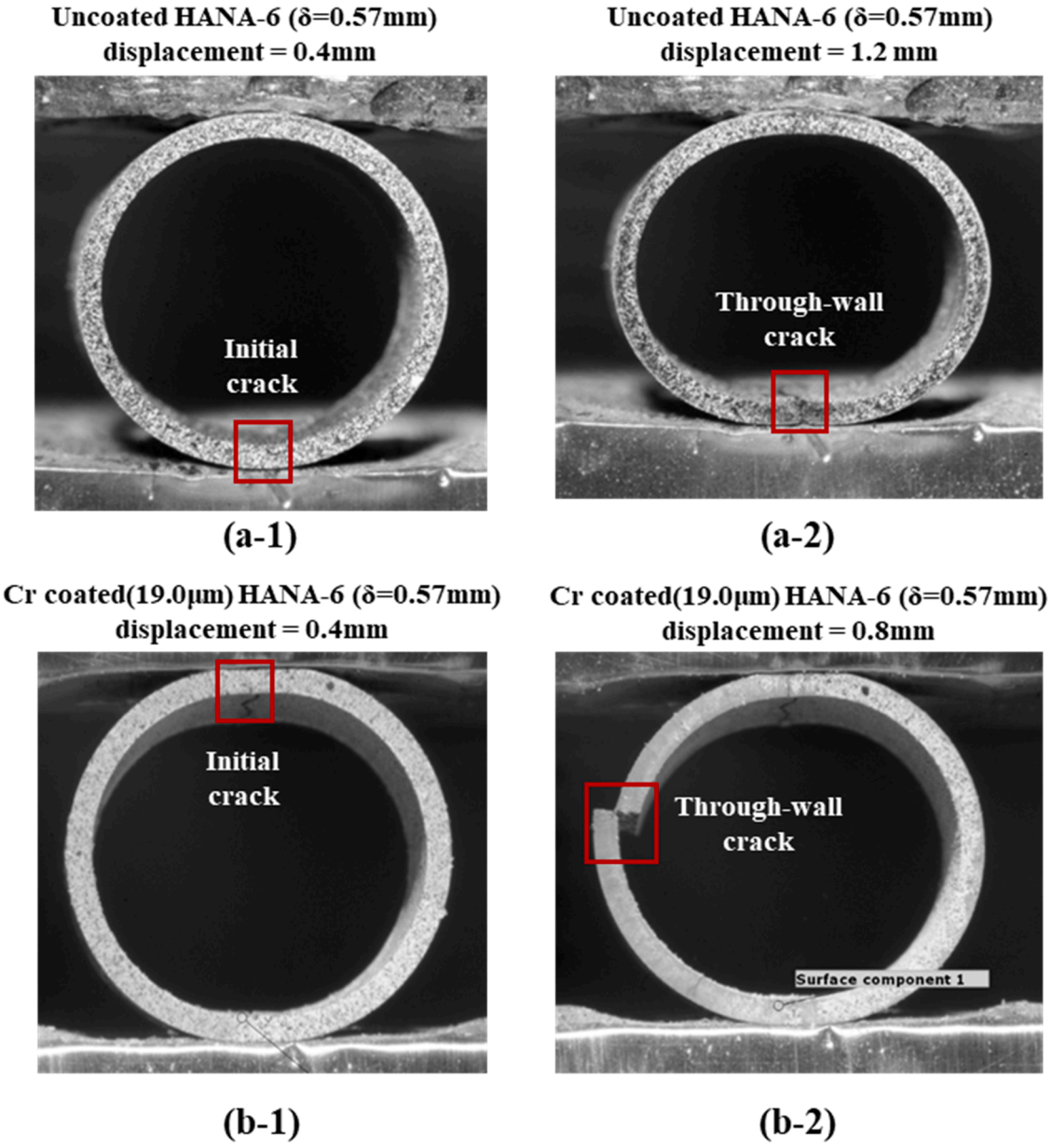

Fig. 7. Crack behavior during RCT. (a-1 and a-2) uncoated HANA-6 with 20 % WG-ECR, (b-1 and b-2) Cr-coated (19.0 μm) HANA-6 with 20 % WG-ECR.

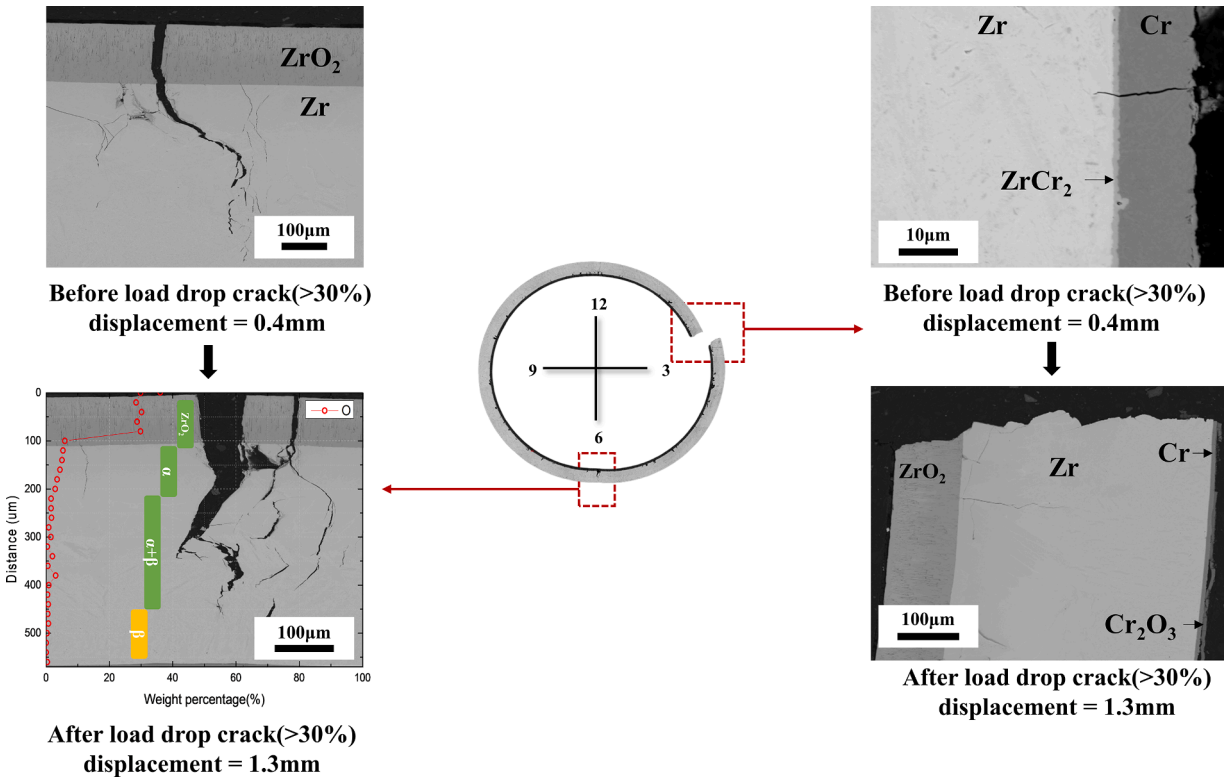

Fig. 8. Cross sectional images at 3 and 6 o'clock right before and after the major load drop and oxygen concentration of Cr-coated (19.0 μm) HANA-6 with 20 % of WG-ECR.

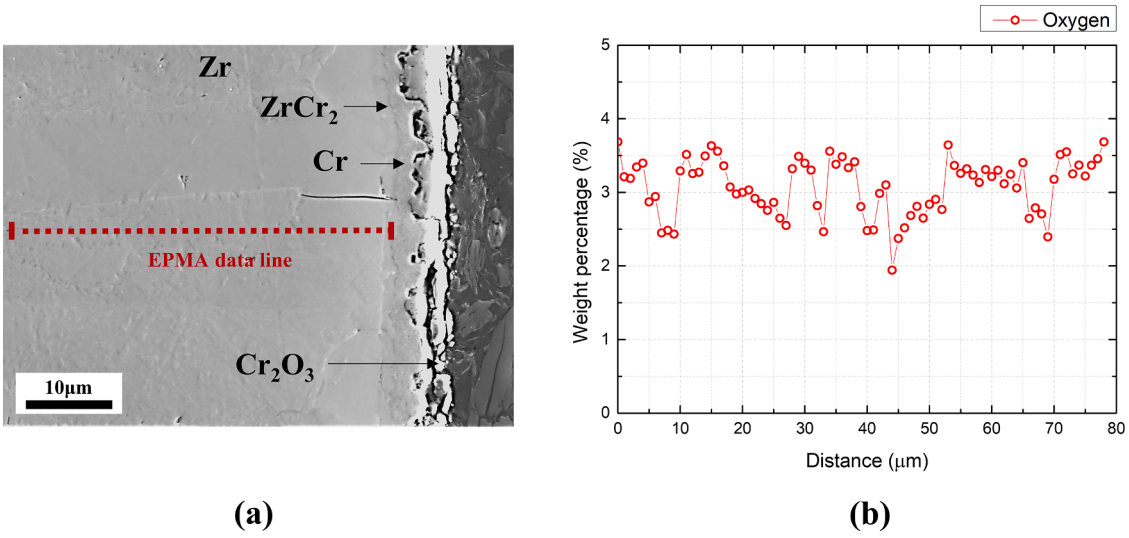

Fig. 9. (a) Cross-sectional image and (b) oxygen concentration of Cr-coated (8.9 μm) HANA-6 at 3′o clock with 20 % WG-ECR.

region at 3′o clock and 9′o clock position experience high level of tensile stresses during RCT. This tensile stress activates cracks developed at $ZrCr_2$ layer and Cr coating to develop into an unstable through-wall crack.

Consequently, the thin cracks developed at $ZrCr_2$ are primarily responsible for the early through-wall crack propagation in comparison with the uncoated Zircaloy cladding. The oxygen underneath the $ZrCr_2$ layer diffused from the coating side. Zr matrix near $ZrCr_2$ layer is brittle alpha phase α(o) characterized with high oxygen concentration above 3 wt.% for the Cr-coated (8.9 μm) HANA-6 (Fig. 9). When sufficient tensile stress is applied, the high oxygen concentration near the $ZrCr_2$ layer promotes the catastrophic fracture by thin cracks developed from $ZrCr_2$ phase.

4.2. *Effect of oxygen diffusion through Cr coating*

Coating thickness changes the rate of oxygen diffusion, thereby affects the oxygen concentration below the $ZrCr_2$ layer. This implies that the thinner coating may exhibit pre-mature ductile-to-brittle transition in comparison with the thicker coating. Fig. 10 shows oxygen

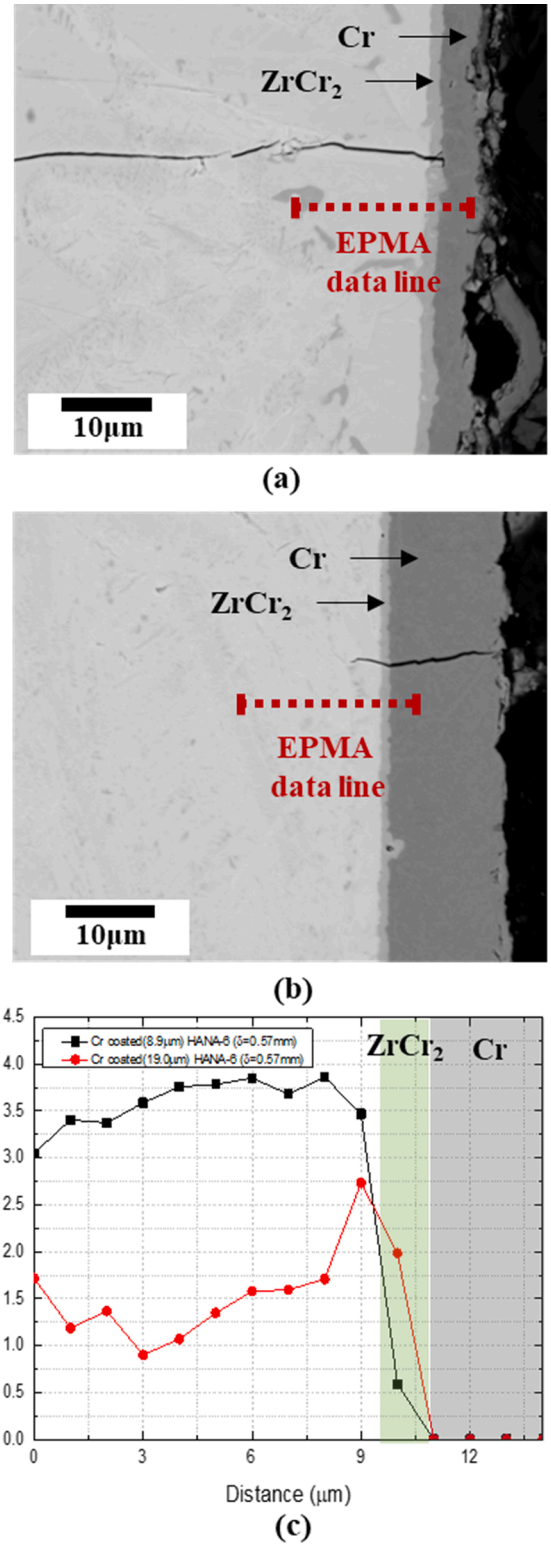

Fig. 10. Crack morphologies and oxygen concentration of Zr substrate near $ZrCr_2$ for Cr-coated HANA-6 with 20 % WG-ECR. (a) Cr coating thickness (8.9 μm), (b) Cr coating thickness (19.0 μm), and (c) oxygen concentration.

concentration of Zr matrix near $ZrCr_2$ layer oxidized to 20 % WG-ECR. The oxygen concentration in Zr matrix for the thinner Cr coating (8.9 μm) is notably higher than that of the thicker coating (19.0 μm). This is because as the Cr coating becomes thicker, the distance that oxygen needs to penetrate to reach the Zr matrix is longer, resulting in a lower oxygen concentration in the Zr matrix.

The different level of oxygen concentration near the $ZrCr_2$ interface resulted in different crack growth behavior. As shown in Fig. 11, when displacement is small (i.e., 0.2 mm), the cracks were observed at or near $ZrCr_2$ layer without further extension. This observation is consistent with past studies reporting that the $ZrCr_2$ layer is more brittle than Zr-alpha(O) [22,23]. For the thinner coating (8.9 μm), With increase of displacement, one can see that the range of the crack spans from the $ZrCr_2$ layer to the Zr matrix. However, for the thicker coating (19.0 μm), the crack's tendency to propagate into the underlying Zr matrix is markedly suppressed, and instead the crack from $ZrCr_2$ layer grows towards the Cr coating. This result indicates that the crack initiated from the $ZrCr_2$ layer propagated to the Cr coating. The presented crack arresting mode of the thicker coating (19.0 μm) is related to the higher Zr matrix ductility associated with the lower oxygen concentration (Fig. 12).

The discussed oxygen distribution and resulting crack growth behavior combinedly affect the RCT behavior. As expected, the Zircaloy cladding with the thinner coating (8.9 μm) undergoes a major load drop earlier than that with the thicker coating (19.0 μm). This provides an explanation to the presented coating thickness sensitivity for ECR limit (Table 2). CrN in Cr/CrN coating (Cr/CrN: 20.1/7.3 μm) decomposes at temperature exceeding 1000 °C, becoming a single Cr layer [24]. This was also confirmed by our study. Hence the role of the CrN layer is considered to merely increase the effective thickness of the Cr coating above 1000 °C. The resultant Cr coating thickness after the decomposition of the CrN layer is ~27 μm. It gives the similar level of ECR limit (Cr/CrN: ECR 19 %, Cr: ECR 20 %) with the cladding coated with 18.8 μm thick Cr as both coatings are thick enough to effectively prevent oxygen diffusion through the coating.

The presence of $ZrCr_2$ precipitates in the Zr matrix formed by further diffusion of Cr into Zr matrix can be another contributor to ductility decrease [15]. Nevertheless, it does not serve as the site for crack initiation; the thin $ZrCr_2$ layer formed beneath to Cr coating is shown to be the primary location of crack propagation under RCT in this study.

4.3. Comprehensive coating thickness effect

It is important to note that when coating thickness is sufficiently thick (i.e., ~40 μm), no appreciable oxygen level was observed beneath the Cr coating layer in a past study as shown in Fig. 13 [7]. In such a case, the major load drop occurred by propagation of cracks from the brittle phases of the inner wall at 6′o clock and 12′o clock. That is, no crack from $ZrCr_2$ was responsible for the observed major drop. Instead, the decrease in the WG-ECR limit (17 % (Uncoated Zircaloy-4) to 14 % (Coated Zircaloy-4 with 39 μm) primarily occurred by the thicker inner-wall oxide (ZrO_2) and oxygen rich α(o) phase for the same ECR due to single side oxidation.

This highlights that the mechanism for the decrease in the ECR limit is different with respect to coating thicknesses: when coating is sufficiently thick, the pre-mature ductile to brittle transition of Cr-coated cladding in terms of ECR occurs primarily by the thicker brittle phase by inner wall oxidation and exhibits no coating sensitivity. It is what the past study by Yook et al. [7] demonstrated. This study unveils that when coating thickness is thin such that appreciable oxygen diffusion occurs during relevant DBA time periods, the cracks developed at $ZrCr_2$ layer becomes responsible for the ECR limit decrease because they can grow into through-wall crack with the high oxygen level near the Zr matrix/$ZrCr_2$ interface and applied tensile stresses during RCT. Coincidentally, the decreases in the ECR limit between the two different mechanisms are similar as ~3 % (ΔECR) on average. Fig. 14 presents a schematic illustration of the coating thickness effect on PQD assessments under RCT.

4.4. Regulatory implications of comprehensive coating design effects

The discussed coating thickness sensitivity may imply the need for

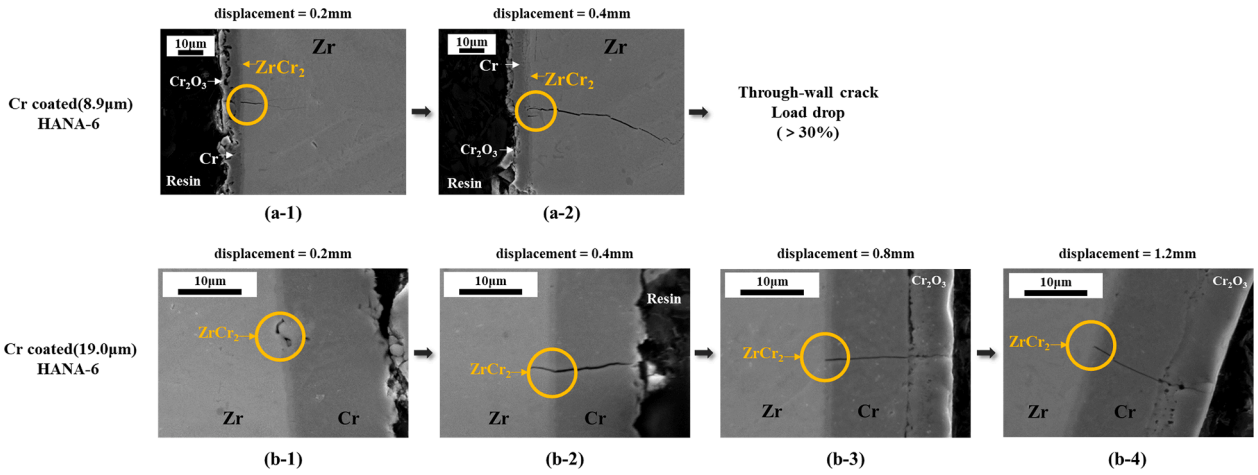

Fig. 11. Crack propagation of the Cr-coated specimens (a) Cr-coated (8.9 μm) HANA-6, (b) Cr -coated(19.0 μm) during RCT.

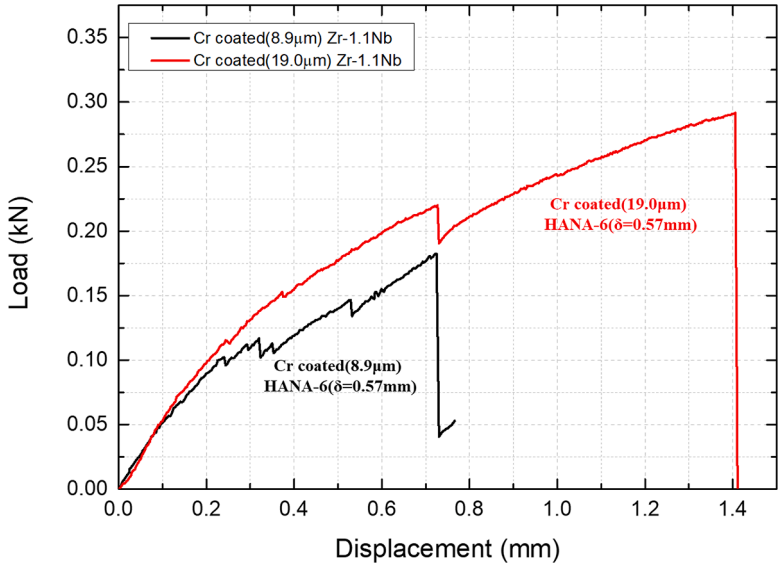

Fig. 12. Load-displacement curves of Cr-coated (8.9 μm) and Cr-coated (19.0 μm) HANA-6 specimens with 20 % WG-ECR.

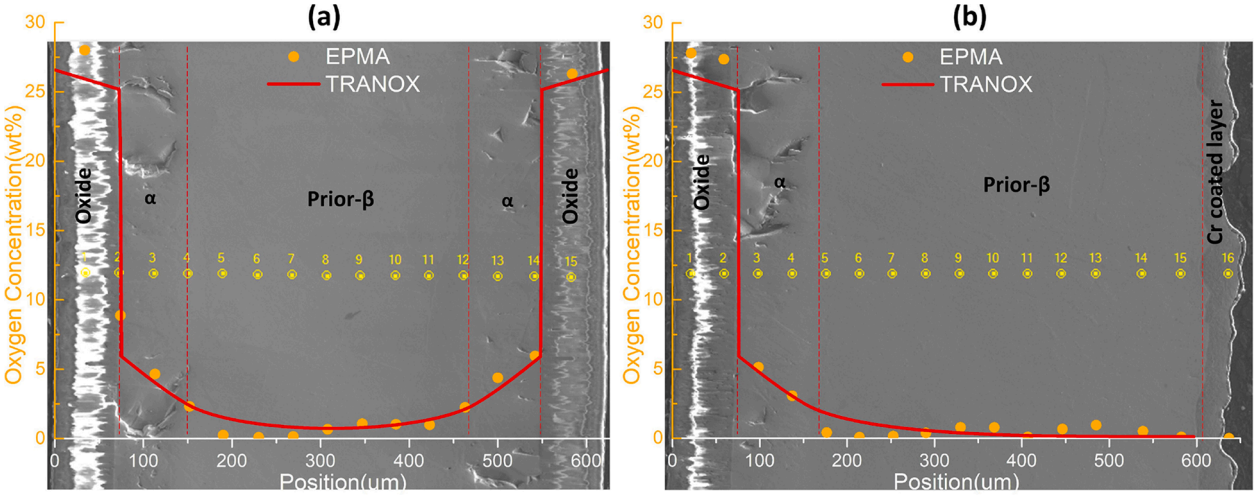

Fig. 13. Comparison of oxygen distributions in Cr-coated (39.6 μm) and uncoated Zircaloy-4.

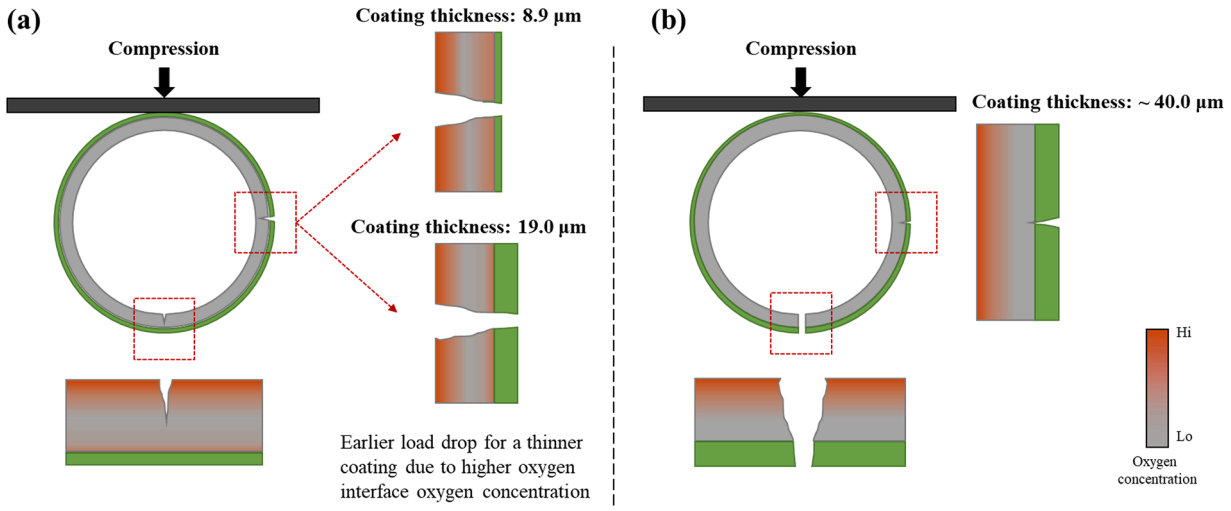

Fig. 14. Schematic diagram for crack propagation modes responsible for major load drop under RCT (a) Cr-coated (8.9 and 19.0 μm) HANA-6, (b) Cr-coated (39.6 μm) Zircaloy-4 [7].

design-specific PQD limits. This is different from the current regulatory approach for the ECCS limit of Zirconium based alloys; most countries, if not all, are adopting universal PQD limits (i.e., 1204 °C and 17 % ECR) regardless of Zircaloy cladding types. It is noteworthy, however, that different Zircaloy cladding types were reported to give different PQD limits. For example, the U.S. NRC reports the CP-ECR limit of 19 % for as-fabricated Zircaloy-4, Zirlo and 20 % for M5 claddings, respectively [25]. Nevertheless, it adopts the most conservative limit and apply it to all cladding materials. By doing so, it can make the regulation simple, yet effective, based on the understanding that a marginal increase in the ECR limit has limited effect on nuclear safety. Making a rational nuclear regulation limit always calls for an elegant, yet conservative, détente of phenomenological complexity and practical implementation. In light of it, it is worthwhile to consider the practical way of addressing the coating design sensitivity in ATF regulation.

Firstly, this study finds no appreciable coating manufacturing effect on high temperature steam oxidation and resulting PQD limits in the tested conditions. Cr coating is subject to recrystallization and grain growth beyond 1100 °C, undergoing significant departure from engineered microstructures and textures [26].

Secondly, this study finds that the PQD limits of the base Zircaloy cladding are transferred onto those of coated claddings. That is, ECR limits of base Zircaloys serve as the ECR ceiling from which ECR reduction for coated cladding occurs. Generally, a higher base Zircaloy ECR limit leads to a higher ECR limit of its Cr-coated cladding. For example, coated Opt. ZIRLO™ and HANA-6 exhibited superior PQD limits compared to coated Zircaloy-4 (Table 2).

Thirdly, this study reveals that thicker coating slightly increases ECR limits by effectively preventing the embrittlement of Zircaloy matrix with oxygen diffusion. However, excessively thick coating layer still

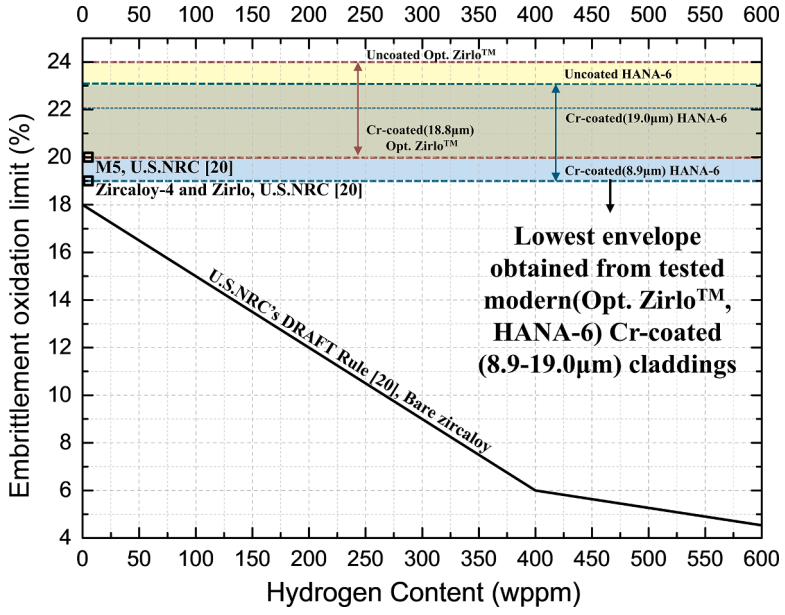

Fig. 15. Comparison of the current ductile to brittle transition ECR [25] and obtained ECR limit(lowest envelope of WG-ECR 19 %) from tested modern(Opt. ZIRLO™, HANA-6) Cr-coated (8.9–19.0 μm) claddings (The horizontal dashed line of Cr coated claddings assumed no hydrogen pickup during steady-state operation).

gives a reduced ECR limit due to the promoted crack propagation from the thicker inner-wall brittle phases under RCT.

Fig. 15 summarizes PQD limits obtained by this study and current ECR limits of bare Zircaloy by U.S. NRC. For the tested base cladding materials (Opt. ZIRLO™ and HANA-6), Cr coating of 8.9 μm, which is substantially thinner than the typical Cr coating thickness (~15–20 μm) under commercialization, can serve as the lowest envelope (ECR 19 %) of ECR limits for tested coated Zircaloys. Hence, ECR limit of 19 % can conservatively serve as the ECR limit for modern base Zircaloy materials (Opt. ZIRLO™ and HANA-6). It shows that the ECR limit of bare Zircaloy cladding decreases due to the hydrogen pickup during steady-state operation. However, the ECR limit of Cr-coated ATF is shown to remain constant because it does not pick up pre-transient hydrogen unless cladding undergoes significant failures in steady-state, highlighting 'hydrogen-independent' ECR limit of Cr-coated ATF. Hence, the figure is intended to highlight the potential advantage of hydrogen-free Cr-coated Zircaloy in terms of allowable ECR limits compared to bare-Zircaloy which inevitably picks up hydrogen with burnup. As such, caution needs to be taken so as not to interpret the horizontal line as 'hydrogen-tolerant' safety limit. It means that Cr-coated cladding does not pickup hydrogen unless the coating undergoes an extended level of unintended structural failure such that its ECR limit is likely to remain constant with burnup as opposed to bare Zircaloy.

5. Conclusion

This study investigated PQD assessments of various Cr-coated cladding designs with respect to base cladding materials, Cr coating methods, and its thickness. The tests were conducted in compliance with the U.S. NRC's PQD test protocols for ECCS criteria. Both inner wall and outer wall of coated (Cr and Cr/CrN) claddings were steam oxidized at ~1204 °C and then water quenched. The post-oxidized specimens were ring compressed to attain offset strains based on which ductility was assessed. The results are further investigated with microstructural analyses. Key findings of this study are as follows:

- ECR limits of coated specimens (Cr and Cr/CrN) are consistently lower than those of the base cladding materials due to the early load drop under RCT. Based on the WG-ECR limit, the reduction ranges from a maximum of 5 % (ΔECR) to a minimum of 1 % (ΔECR). Yet, time needed to reach the ECR limit is still increased for coated specimens because it effectively undergoes single-side oxidation with protective coating.
- Cracks initiated from $ZrCr_2$ at 3′o clock and 9′o clock are primarily responsible for the early major load drop observed for tested coating thicknesses (8.9 μm and 19.0 μm), and hence resulted in the reduced ECR limits. The cracks from $ZrCr_2$ were promoted by an increased oxygen concentration of the interfacing Zr matrix owing to the diffusion of oxygen through the coating. The thicker coating reduces this oxygen level, thereby delaying the load drop from $ZrCr_2$ during RCT and increases the ECR limit. However, a coating sufficiently thick (i.e., 39.4 μm) to prevent oxygen diffusion undergoes a different failure mode under RCT; a major load drop is occurred by cracks propagated from the brittle phases of the inner wall at 6′o clock and 12′o clock [7]. Coincidentally, the level of the ECR decrease for this mode of major load drop is similar to that of the $ZrCr_2$-induced major load drops which are relevant to the thinner coatings (i.e., 8.9 μm and 19.0 μm)
- The maximum attainable ECR limit of coated ECR limits is affected by the base Zircaloy as it gives as the ECR ceiling from which ECR reduction for coated cladding occurs. For the tested base cladding materials (Opt. ZIRLO™ and HANA-6), ECR 19 %, which is the limit for Cr-coated (8.9 μm) HANA-6, may serve as the lower envelope limit. Hence, ECR 19 % can conservatively serve as the conservative, yet non-design specific, Cr-coated ECR limit for the most of the modern base Zircaloy materials (Opt. ZIRLO™ and HANA-6).

CRediT authorship contribution statement

SungHoon Joung: Writing – review & editing, Writing – original draft, Visualization, Validation, Methodology, Investigation, Formal analysis, Data curation, Conceptualization. **Jinsu Kim:** Methodology, Investigation, Formal analysis, Data curation. **Martin Ševeček:** Resources, Data curation. **Juri Stuckert:** Resources, Data curation. **Youho Lee:** Writing – review & editing, Writing – original draft, Supervision, Resources, Project administration, Methodology, Investigation, Funding acquisition, Data curation, Conceptualization.

Declaration of competing interest

The authors declare that they have no known competing financial interests or personal relationships that could have appeared to influence the work reported in this paper.

Data availability

No data was used for the research described in the article.

Acknowledgment

This work was supported by the Nuclear Safety Research Program through the Korea Foundation of Nuclear Safety (KoFONS) using the financial resource granted by the Nuclear Safety and Security Commission (NSSC) of the Republic of Korea [2101051 (50 %)] and [00241683 (50 %)]. This work was conducted in the frame of IAEA's Coordinated Research Project on Testing and Simulation for Advanced Technology and Accident Tolerant Fuels (ATF-TS T12032). This work was supported by the Institute of Engineering Research at Seoul National University.

Appendix

Fig. A shows the offset strain of Zircaloy-4 ($\delta = 0.57$ mm) with WG-EGR was obtained in this study with the U.S. NRC's past results. The result exhibits remarkable agreement with that of U.S. NRC's experimental data [1].

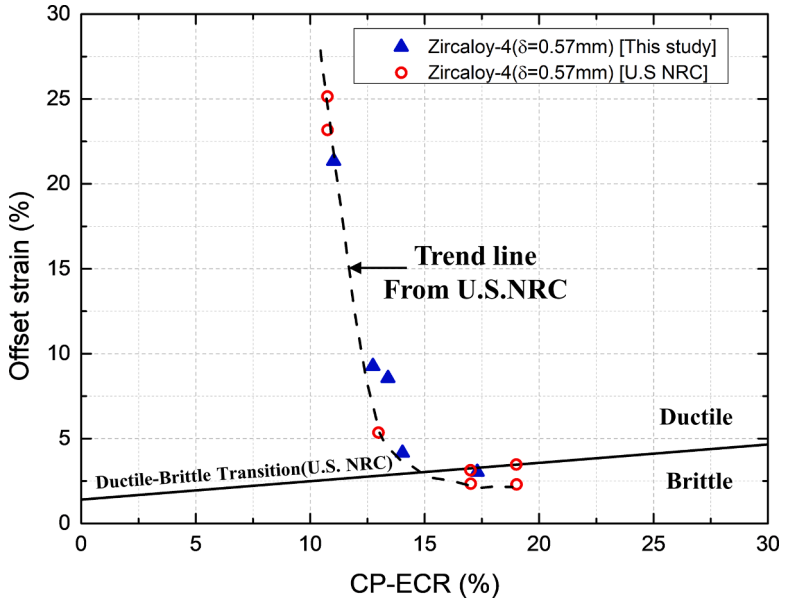

Fig. A. CP-ECR to offset strain curve for Zircaloy-4 (δ 0.57 mm) with the U.S. NRC's past result [1].

Fig. B shows the stress distribution of cladding with fairly cylindrical shape during RCT, as obtained through FEA using Abaqus. Detailed method for finite element modeling of RCT can be found in Kim et al. [27]. Moreover, according to the FEA code calculations, the maximum hoop stress reaches 721 [MPa] at the 6 o'clock and 12 o'clock inner wall positions. At the outer regions at the 3 o'clock and 9 o'clock positions, the tensile stress levels are slightly lower at 670 [MPa] compared to the outer wall positions at 6 o'clock and 12 o'clock. Despite the lower hoop stress at the 3 o'clock and 9 o'clock positions compared to the hoop stress at 6 o'clock and 12 o'clock, crack propagation in coated cladding initiates from the $ZrCr_2$ layer on the outer walls at 3 o'clock and 9 o'clock due to its higher brittleness compared to ZrO_2.

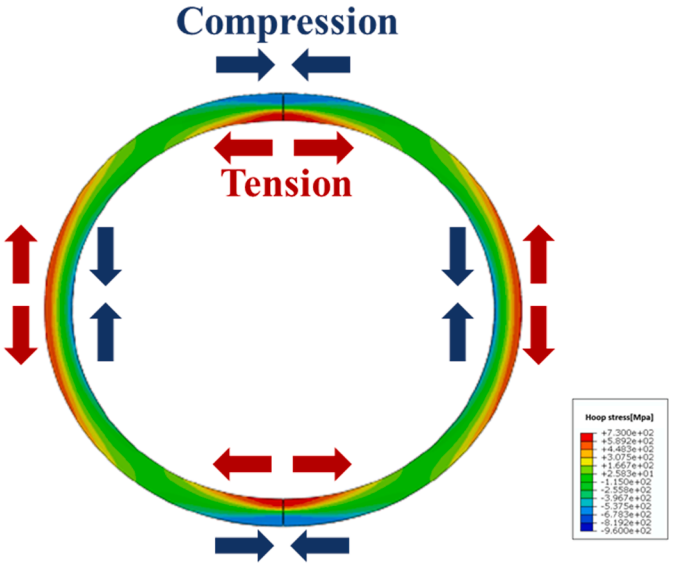

Fig. B. Stress distribution of cladding with a fairly cylindrical shape during RCT simulated by FEA.

Fig. C shows the cross-sectional images of all types of claddings after oxidation in this study. From the Fig. C, thickness of ZrO_2 at the inner wall can be readily measured and is reported in Table 2. $ZrCr_2$ layer was observable in SEM and its thicknesses were measured. 60 different locations were analyzed for inner ZrO_2, $ZrCr_2$, and Cr thickness, and their average and standard deviations are summarized in Table 2.

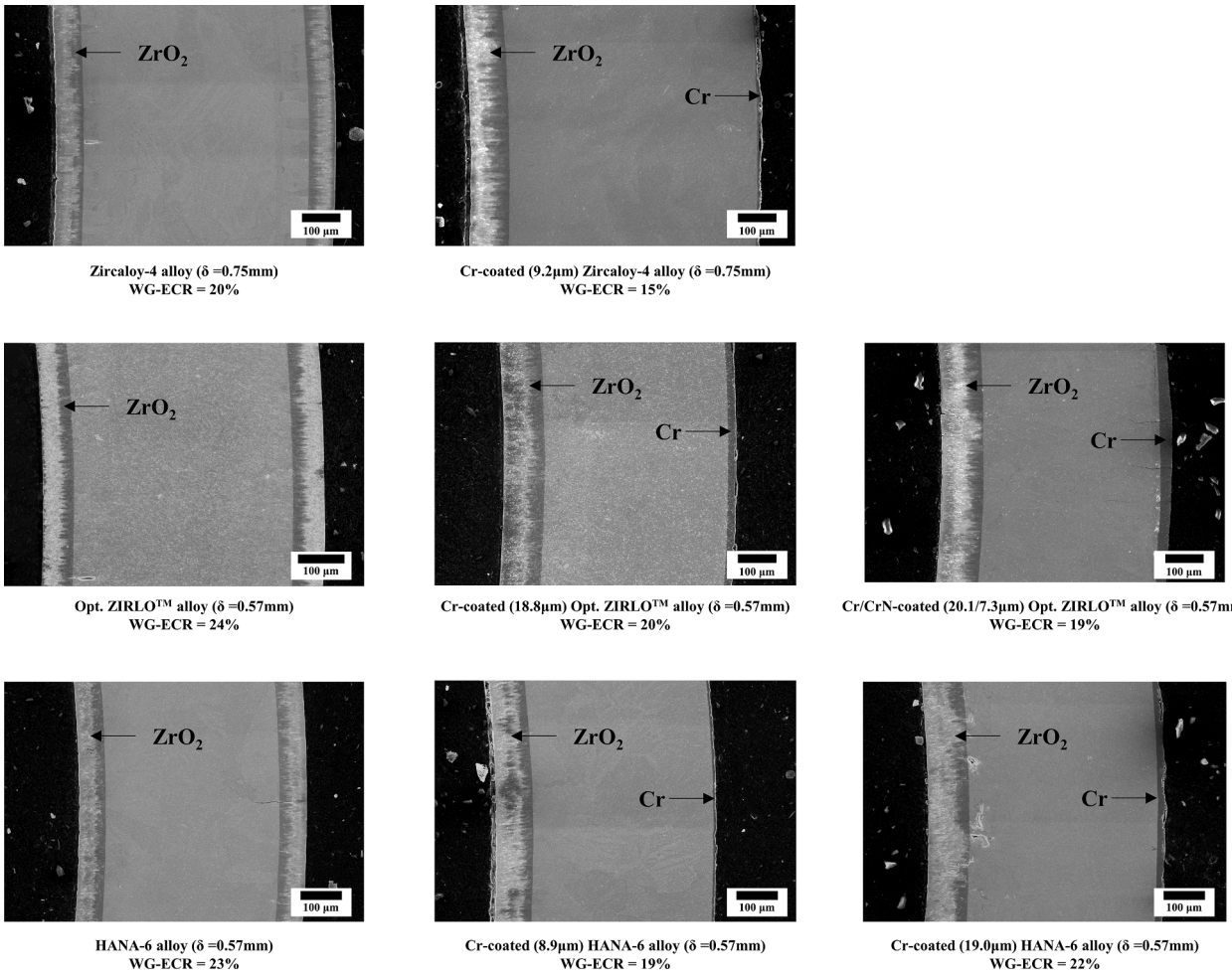

Fig. C. Cross-sectional images of post-steam oxidized cladding materials.

Fig. D exhibits SEM images of post-steam oxidized HANA-6 and Cr-coated (19.0 μm) HANA-6 with associated EPMA and calculated TRANOX oxygen profiles. Thickness of ZrO_2 was compared with prediction of TRANOX-2.0 [11], and they are in good agreement as shown in Fig. D. Hence, the thickness of the inner Zr-alpha(O) was obtained from TRANOX.

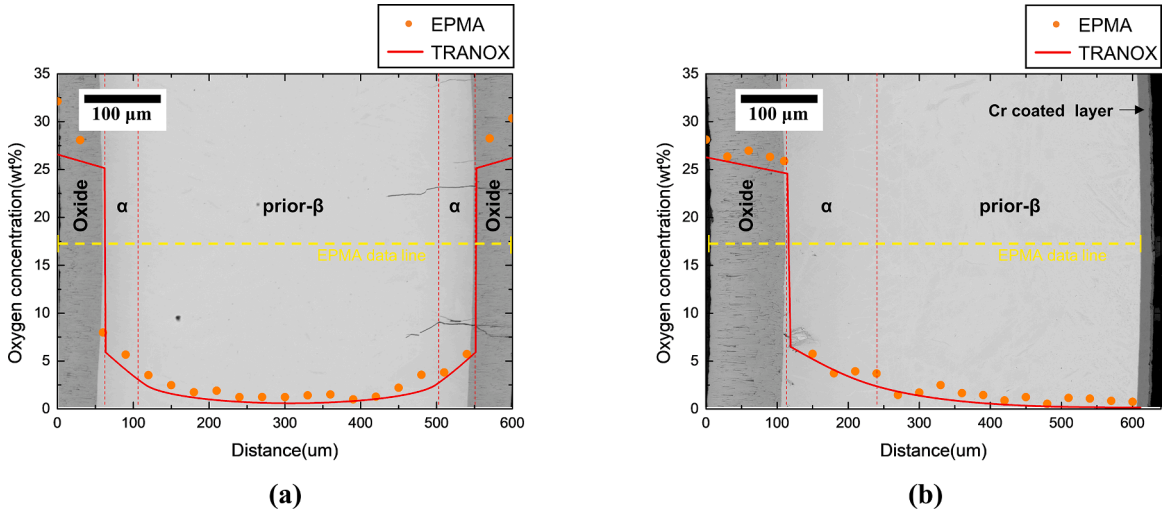

Fig. D. SEM images of post-steam oxidized cladding materials with associated EPMA and calculated TRANOX oxygen profiles: (a) Uncoated HANA-6 (ECR 20 %); (b) Cr-coated (19.0 μm) HANA-6 (ECR 20 %).

References

[1] ``NUREG/CP-6967-Cladding Embrittlement During Postulated Loss-of-Coolant Accidents" U.S.NRC, 2008.

[2] D. Hobson, Ductile-Brittle Behavior of Zircaloy Fuel Cladding, Oak Ridge National Lab., Tenn., 1972.

[3] D. Hobson, P. Rittenhouse, Embrittlement of Zircaloy-Clad Fuel Rods by Steam During Loca Transients, Oak Ridge National Lab., Tenn., 1972.

[4] J. Yang, et al., Review on chromium coated zirconium alloy accident tolerant fuel cladding, J. Alloys Compd. 895 (2022) 162450.

[5] K.A. Terrani, Accident tolerant fuel cladding development: promise, status, and challenges, J. Nucl. Mater. 501 (2018) 13–30.

[6] U.S.NRC, Supplemental Guidance Regarding the Chromium-Coated Zirconium Alloy Fuel Cladding Accident Tolerant Fuel Concept, Interim Staff Guidance, 2020. ATF-ISG-2020-01.

[7] H. Yook, K. Shirvan, B. Phillips, Y. Lee, Post-LOCA ductility of Cr-coated cladding and its embrittlement limit," (in English), J. Nucl. Mater. 558 (2022) 153354.

[8] ``Acceptance criteria for emergency core cooling systems for light water cooled nuclear power reactors,'' and Appendix K to 10 CFR 50. "ECCS Evaluation Models, U.S. Federal Register 39 (3)," vol. 10 CFR 50.46, 1974.

[9] S. Bang, Y. Lee, The statistical ductility of embrittled Zircaloy-4 and its regulatory implications, J. Nucl. Mater. 554 (2021) 153085.

[10] K. Keum, Y. Lee, Effect of cooling rate on the residual ductility of post-LOCA Zircaloy-4 cladding, J. Nucl. Mater. 541 (2020) 152405.

[11] D. Kim, H. Yook, K. Keum, Y. Lee, TRANOX: model for non-isothermal steam oxidation of Zircaloy cladding, J. Nucl. Mater. 556 (2021) 153153.

[12] H. Yook, Y. Lee, Post-LOCA ductility assessment of Zr-Nb Alloy from 1100 °C to 1300 °C to explore variable peak cladding temperature and equivalent cladding reacted safety criteria, J. Nucl. Mater. 567 (2022) 153829.

[13] "USNRC. Regulatory guide 1.223-determing post quench ductility," Washington. D. C., USA, 2018.

[14] S. Kim, J.-H. Kang, Y. Lee, Suppressed hydride precipitation in the welding zone of a zirconium-based alloy cladding tube, J. Nucl. Mater. 580 (2023) 154406.

[15] D. Kim, Y. Lee, Diffusion of chromium of Cr-coated Zircaloy accident tolerant fuel cladding: model development and experimental validation, Surf. Coat. Technol. 468 (2023) 129698.

[16] D. Kim, M. Ševeček, Y. Lee, Characterization of eutectic reaction of Cr and Cr/CrN coated Zircaloy accident tolerant fuel cladding, Nucl. Eng. Technol. 55 (2023) 3535–3542.

[17] R. Pawel, J. Cathcart, R. McKee, The kinetics of oxidation of Zircaloy-4 in steam at high temperatures, J. Electrochem. Soc. 126 (7) (1979) 1105.

[18] J. Brachet, et al., Evaluation of equivalent cladding reacted parameters of Cr-coated claddings oxidized in steam at 1200 °C in relation with oxygen diffusion/partitioning and post-quench ductility, J. Nucl. Mater. 533 (2020) 152106.

[19] J.-C. Brachet, et al., Early studies on Cr-coated Zircaloy-4 as enhanced accident tolerant nuclear fuel claddings for light water reactors, J. Nucl. Mater. 517 (2019) 268–285.

[20] T.S. Byun, E. Lara-Curzio, R.A. Lowden, L.L. Snead, Y. Katoh, Miniaturized fracture stress tests for thin-walled tubular SiC specimens, J. Nucl. Mater. 367 (2007) 653–658.

[21] S. Lumley, S. Murphy, P. Burr, R. Grimes, P. Chard-Tuckey, M. Wenman, The stability of alloying additions in zirconium, J. Nucl. Mater. 437 (1–3) (2013) 122–129.

[22] J. Jiang, M. Du, Z. Pan, M. Yuan, X. Ma, B. Wang, Effects of oxidation and inter-diffusion on the fracture mechanisms of Cr-coated Zry-4 alloys: an in situ three-point bending study, Mater. Des. 212 (2021) 110168.

[23] J.-S. Jiang, D.-Q. Wang, M.-Y. Du, X.-F. Ma, C.-X. Wang, X.-J. He, Interdiffusion behavior between Cr and Zr and its effect on the microcracking behavior in the Cr-coated Zr-4 alloy, Nucl. Sci. Tech. 32 (12) (2021) 134.

[24] J. Liu, et al., Oxidation behavior, thermal stability, and the coating/substrate interface evolution of CrN-coated Zircaloy under high-temperature steam, Corros. Sci. 185 (2021) 109416.

[25] U.S.NRC., "Establishing Analytical Limits for Zirconium-Alloy Cladding Material," in "Regulatory Guide," U.S. Nuclear Regulatory Commission (U.S. NRC), March 2014, vol. Regulatory Guide 1.224.

[26] S. Johnstone, F. Henderson, H. Wain, Recrystallization and the ductility of chromium, Nature 180 (4590) (1957) 806.

[27] J. Kim, S. Joung, Y. Lee, Effect of Cr coating on the mechanical integrity of accident tolerant fuel cladding under ring compression test, J. Nucl. Mater. 585 (2023) 154603.